Available online at www.sciencedirect.com

SciVerse ScienceDirect

Journal of the European Ceramic Society 32 (2012) 2035–2042

www.elsevier.com/locate/jeurceramsoc

Characterisation of the microstructure and thermal properties of $Nd_2Zr_2O_7$ and $Nd_2Zr_2O_7$/YSZ thermal barrier coatings

G. Moskal [a,*], L. Swadźba [a], M. Hetmańczyk [a], B. Witala [a], B. Mendala [a], J. Mendala [b], P. Sosnowy [c]

[a] *Silesian University of Technology, Department of Materials Science, 40-019 Katowice, Slaskie, Poland*
[b] *Silesian University of Technology, Department of Materials Technology, 40-019 Katowice, Slaskie, Poland*
[c] *Factory of Transport Equipment WSK "PZL – Rzeszów" Stock Company, Poland*

Received 23 July 2011; received in revised form 2 December 2011; accepted 5 December 2011
Available online 9 January 2012

Abstract

The microstructure of following thermal barrier coatings (TBC) was characterised in this paper: monolayer coatings $Nd_2Zr_2O_7$ and 8YSZ; a double ceramic layered (DCL) coating. Coatings were characterised by thicknesses that did not exceed 300 μm and porosities of approx. 5%. The chemical and phase composition analysis of the DCL layers revealed an external $Nd_2Zr_2O_7$ ceramic layer approx. 80 μm thick, a transitional zone approx. 120 μm thick and an internal 8YSZ layer 100 μm thick. For the case of the monolayer coating, the $Nd_2Zr_2O_7$ pyrochlore phase was the only one-phase component. The surface topography of both TBC systems was typical for plasma sprayed coatings, and compressive stress state had a value of approx. 5–10 MPa. Measurements of the thermal parameters, i.e., thermal diffusivity, point to considerably better insulative properties for both new types of layers when compared to the standard 8YSZ layers.

Keywords: Thermal conductivity; Engine components; Functional applications

1. Introduction

Thermal barrier coatings (so-called *TBCs*) are examples of protective coatings, such as used in gas turbines, and these coatings are the most advanced when considering their material and technological qualities. They are characterised by perfect insulating properties. The insulative behaviour lowers the temperature of the part (approx. 170 °C), which is subjected to creep due to the hot temperatures in certain engine section (e.g., combustion chambers, guiding vanes and rotating vanes), to a temperature range that promotes a long-lasting and safe service life under high operating temperatures. Application of such a protective coating extends the lives of the elements three or four times, while at the same time, reducing fuel consumption.[1] Thermal barrier coatings have been used for approx. 40 years, and they are based on the formation of an outer ceramic layer, approx. 250 μm. This layer is usually composed of zirconium oxide modified with yttrium oxide (8YSZ–$ZrO_2 \times 8Y_2O_3$). Because the ceramic layer is prone to cracking and falling off, additional prime layers of Ni(Co)CrAlY or NiAl(Pt) are applied.[2]

Although such layers have been used for several years, their durability is still a fundamental problem. Because of this issue, intensive research has been carried out that aims to replace the 8YSZ oxide with a new type of ceramic material that will surpass it in properties and durability. The scope of most of the research has concentrated on compositions based on the ZrO_2 phase, modified with one or two rare earth element type oxides (RE_2O_3), but different from Y_2O_3. Rare earth zirconates with the pyrochlore-type structure and a general formula of $RE_2Zr_2O_7$ are other types of materials that have been tested.

Several independent works[3–16] led to a common conclusion: rare earth zirconates with a general formula $RE_2Zr_2O_7$, which crystallize with an ordered pyrochlore-type structure, are a promising group of materials for use as TBC ceramic layers. Experiments revealed that the $La_2Zr_2O_7$ compound (porosity 3%) demonstrated thermal conductivity on the order of 1.6 $Wm^{-1} K^{-1}$, while the 8YSZ oxide (8.8% porosity) had a value of 2.5 $Wm^{-1} K^{-1}$. The use of $M_2D_2O_7$-type compounds – where M stands for Gd, La, and Y; D stands for Hf, Ti, and Zr – was proposed as well. A concept to apply a compound of the

* Corresponding author.
E-mail address: grzegorz.moskal@polsl.pl (G. Moskal).

0955-2219/$ – see front matter © 2011 Elsevier Ltd. All rights reserved.
doi:10.1016/j.jeurceramsoc.2011.12.004

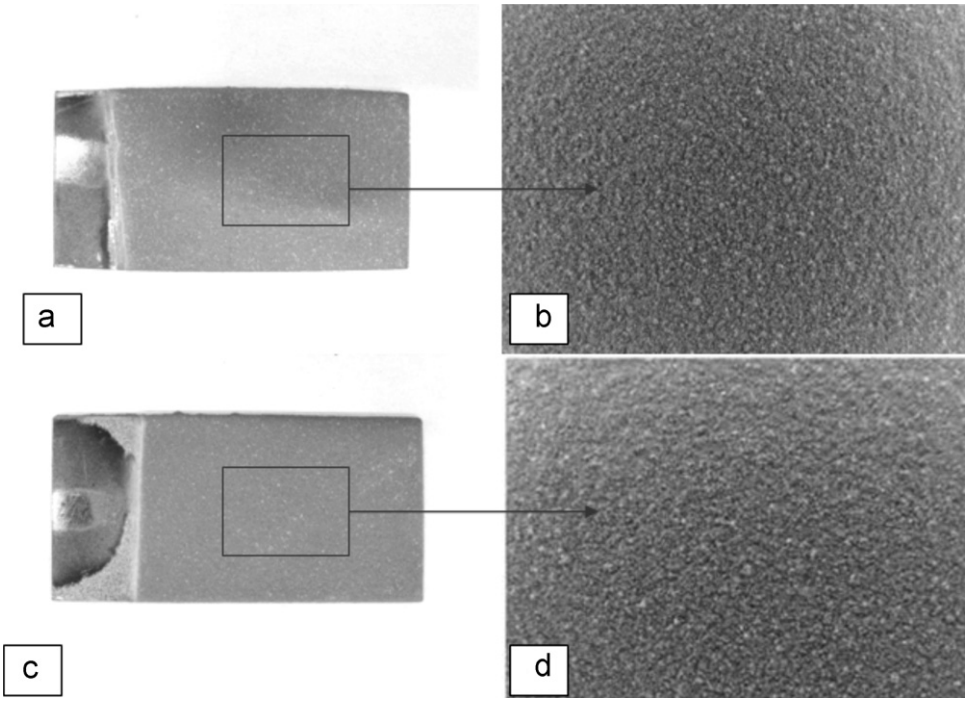

Fig. 1. Macroscopic view of the TBC layer: type $Nd_2Zr_2O_7$ (a), surface details are visible with a stereo microscope – magnification 32× (b), the $Nd_2Zr_2O_7$/8YSZ DLC layer (c) and (d) and analogous to the $Nd_2Zr_2O_7$ specimen, details of the surface are visible through the stereo microscope – magnification 32×.

similar type also was proposed, but the M component comprises elements of the lanthanide group from La to Yb.

2. Experimental procedure

The TBC was obtained through plasma spraying the $Nd_2Zr_2O_7$ ceramic powder as a monolayer and as a DCL layer with an additional 8YSZ ceramic layer (the zirconate layer) that separates it from the prime layer. A nickel superalloy (AMS 5599) was used as the base alloy, and a NiCrAlY bondcoat was sprayed on its surface. The alloy base was 2 mm thick, and the NiCrAlY layer was approx. 125 μm. A prime layer and an outer ceramic layer were sprayed by the APS (*atmospheric plasma spraying*) method at standard process parameters. Detailed results of the tests, which characterised the microstructure, technological properties and thermal properties of the prime and ceramic powders, are presented in those papers.[17–19]

The scope of tests comprised

- macroscopic visual inspection of sprayed flat samples;
- macroscopic examination of the surface with a stereo microscope (SZX9, produced by the Olympus Company, in a magnification range from 6.3× to 40×);
- characterisation of the surface and analysis of the geometrical surface parameters to analyse the topography of the outer ceramic layer (MicroProf contactless optical profilometer, produced by the FRT Company);
- evaluation of the surface with a scanning electron microscope SEM (Hitachi model S-3400 N);
- determination of the phase composition and estimation of the stress state in the ceramic layer by the $\sin^2\Psi$ method coupled by XRD (*X-ray diffraction*) method with a Roentgen diffraction instrument (JEOL JDX-7S) and an EBSD (*electron backscatter diffraction*) detector, which was attached to the Hitachi S-3400 N microscope;
- evaluation of the microstructure of the TBC system as well as with the thickness characteristics, quantitative and qualitative characteristics and porosity characteristics of the ceramic layer. Observations were performed on a digital camera system (Olympus DP70) and a scanning electron microscope (Hitachi S-4200). Qualitative and quantitative evaluations were carried out with a program that provided for the

Table 1
Results from the quantitative roughness analysis of the TBC layers, $Nd_2Zr_2O_7$ and $Nd_2Zr_2O_7$/8YSZ.

	$Nd_2Zr_2O_7$	$Nd_2Zr_2O_7$/8YSZ
Rz [μm]	46.2	41.6
Ra [μm]	8.87	7.58
Rq [μm]	10.9	9.32

Rz: max height of profile of roughness, Ra: mean arithmetic deviation of profile of roughness, Rq: mean square deviation of profile of roughness.

Table 2
Thickness measurement results for the prime and ceramic layers in the TBC system.

Thickness [μm]	NiCrAlY	$Nd_2Zr_2O_7$	$Nd_2Zr_2O_7$/8YSZ
Average value	125	240	300
Max. value	156	277	321
Min. value	110	189	287
Standard dev.	7	12	14

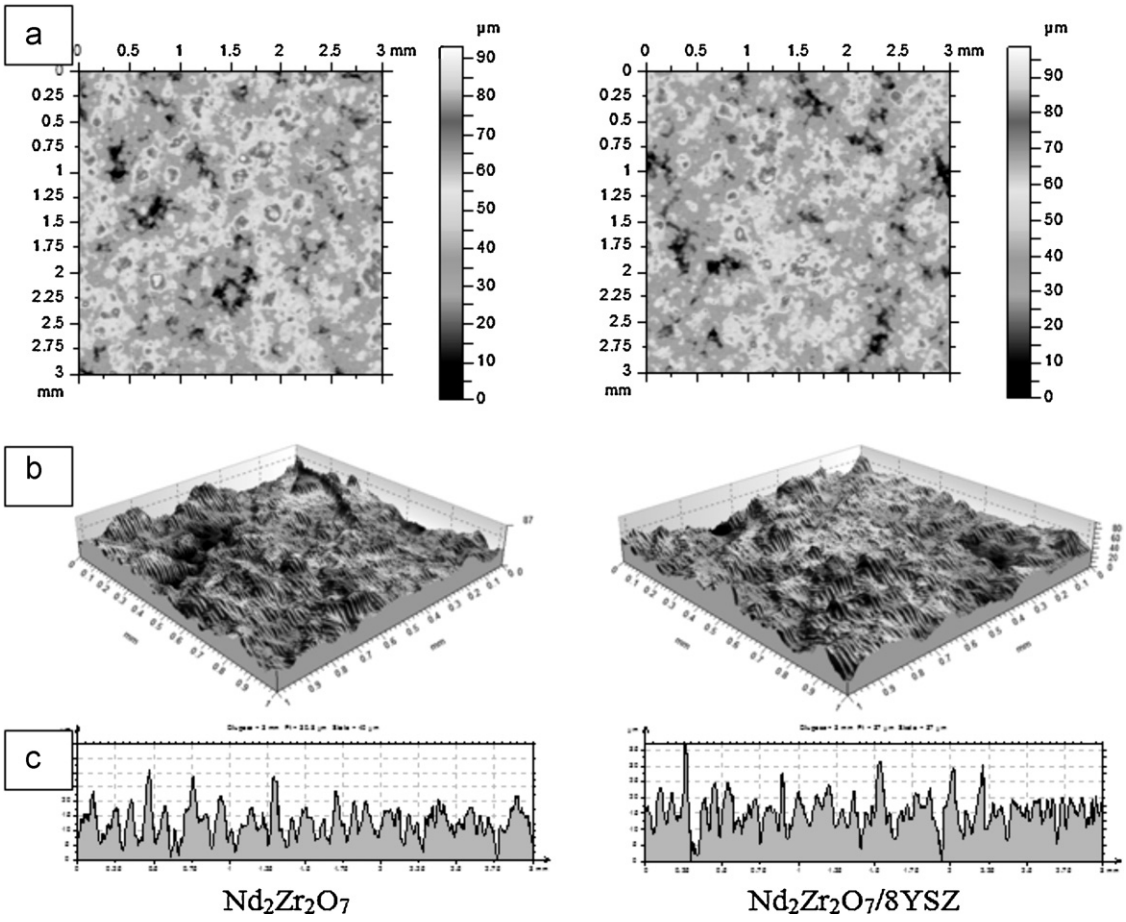

Fig. 2. Geometrical surface configuration of the TBC layer types $Nd_2Zr_2O_7$ and $Nd_2Zr_2O_7$/8YSZ represented by a 2D isometric image (a), 3D topographical map (b) and distribution of the roughness (c).

automatic analysis of the "MetIlo" image (J. Szala – Silesian University of Technology);

- determination of the chemical composition by microanalysis through the EDS (*energy-dispersive spectroscopy*) method with a software program (produced by the Thermo Scientific System Seven Company) on the Hitachi S-4200;
- determination of the thermal diffusivity of the TBC layers was conducted by the L-F (*laser-flash*) method on an LFA 427 (Netzsch Company). This method directly measured the thermal diffusivity in a temperature range of 20–1100 °C under an argon atmosphere on square samples 10 mm × 10 mm × 2 mm. The base material, base material with a bondcoat and the base material with both a bondcoat and an outer ceramic layer were the subjects of the tests. To calculate the thermal diffusivity value of the whole TBC system, Cowan's model was used. Then, the bilayer model was used to determine the thermal diffusivity of the bondcoat (at known thermal diffusivity of the AMS5599 base material)

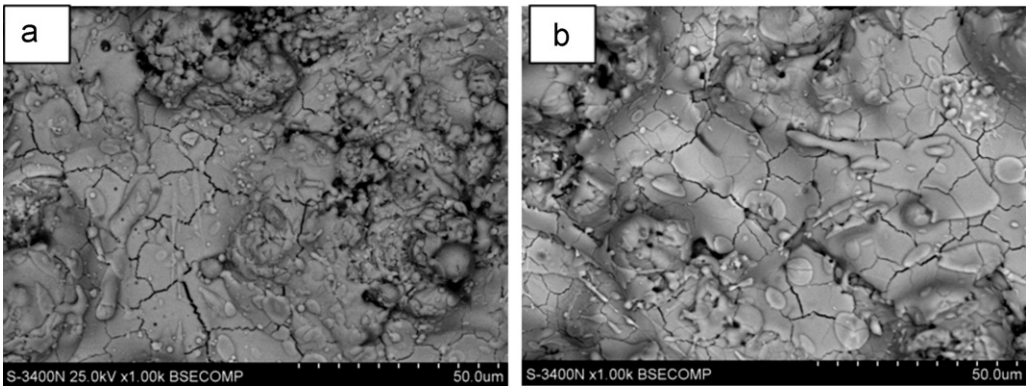

Fig. 3. Surface morphologies of the TBC layers, types $Nd_2Zr_2O_7$ (a) and $Nd_2Zr_2O_7$/8YSZ (b).

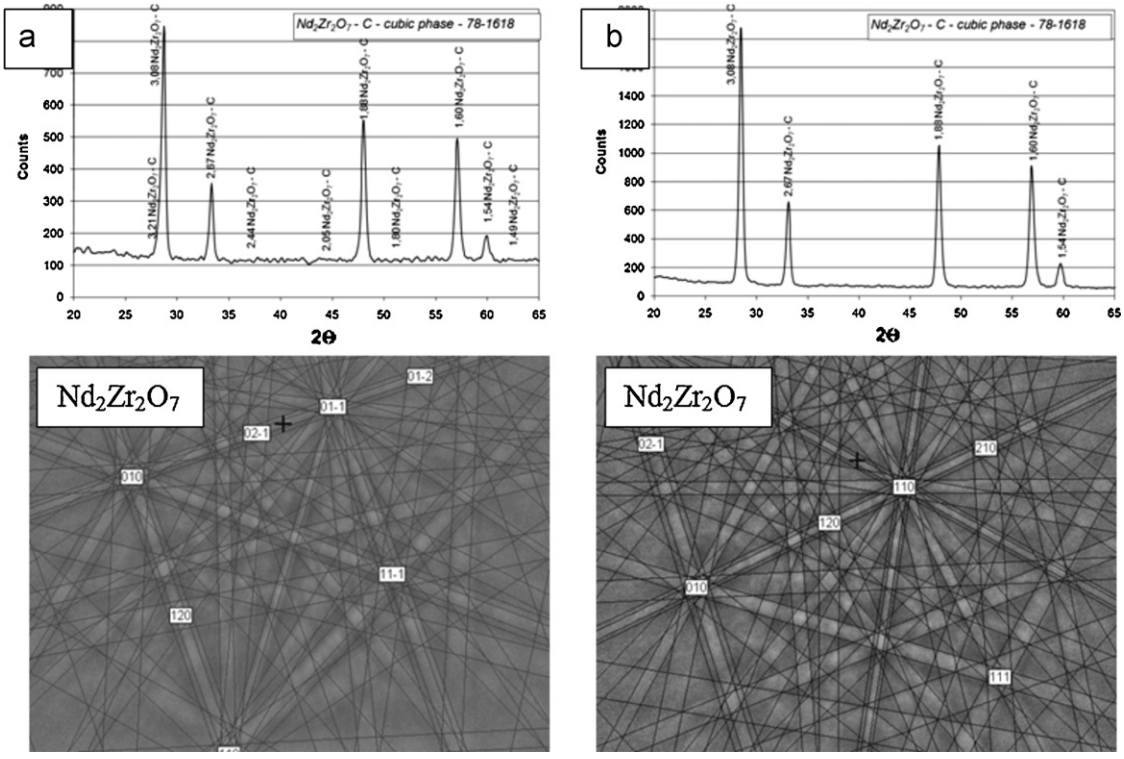

Fig. 4. Phase composition results, carried out on the surface of the TBC layer types $Nd_2Zr_2O_7$ (a) and $Nd_2Zr_2O_7$/8YSZ (b).

and the ceramic layer; the thermal diffusivity for the base plus bilayer was taken as a reference parameter; and

- determination of an analytical value of the coefficient of thermal diffusivity, as a function of temperature, based on the thermal diffusivity measurement results and the specific heat and coefficient of linear expansion values for the charge powders.[17–19]

3. Results and discussion

The macroscopic visual inspection of both sprayed TBC layers revealed that the applied APS process parameters enabled the formation of a coating of satisfactory quality. The outer ceramic layer was homogeneous in thickness, and defect free. The appearance of the outer ceramic surface is typical for these types of coatings. The olive green colour of both coatings was due to the olive green colour of the charge powder. Example images, showing $Nd_2Zr_2O_7$ and $Nd_2Zr_2O_7$/8YSZ TBC layers, are presented in Fig. 1.

As expected, a more detailed description of the surface topography was obtained with a contactless optical profilograph where quantitative parameters, which characterise the topography of the outer ceramic layer, were obtained as well. The geometrical shape of a selected section of the tested surface (1.0 mm × 1.0 mm) is represented by a 2D isometric image, a 3D topographical map and a distribution of the roughness for both types of layers, as shown in Fig. 2(a), (b) and (c), respectively. Results of the quantitative tests, which characterised the surface geometry of the ceramic layer, are presented in Table 1. From the surface configuration maps and results, one can conclude that the estimated $Nd_2Zr_2O_7$ and $Nd_2Zr_2O_7$/8YSZ layers are characterised by a structure that is typical for ceramic layers fabricated by plasma spraying.

In order to obtain a more complete evaluation, the surface state of the TBC sprayed layers and the morphology of the top layer must be characterised as well. The structure and presence of cracks, which are perpendicular to the base surface, also should

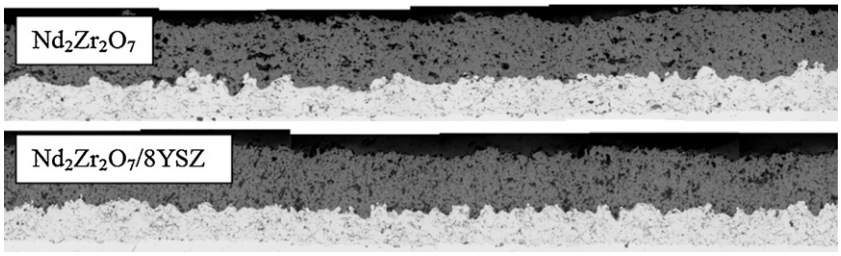

Fig. 5. Macroscopic view of the TBC layers, types $Nd_2Zr_2O_7$ and $Nd_2Zr_2O_7$/8YSZ.

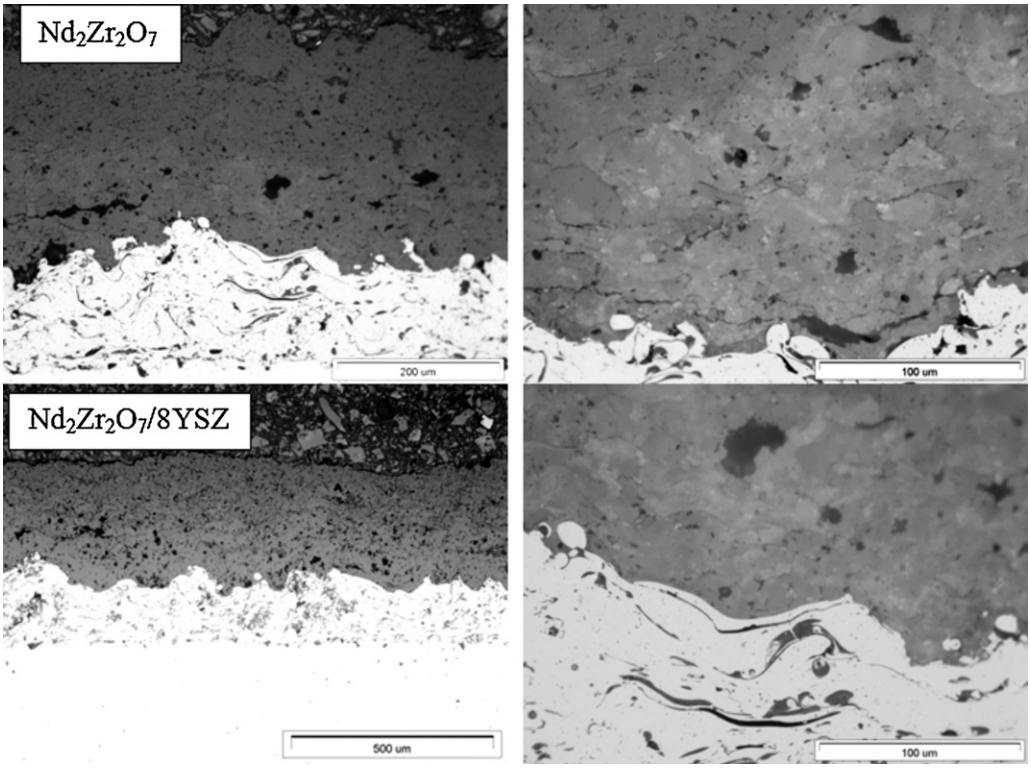

Fig. 6. Details of the structure of the TBC inner layer, types $Nd_2Zr_2O_7$ and $Nd_2Zr_2O_7$/8YSZ.

be considered, as these cracks are visible along grain boundaries. Example photos, taken by the SEM method, from the top ceramic $Nd_2Zr_2O_7$ and $Nd_2Zr_2O_7$/8YSZ coating layer surfaces are presented in Fig. 3.

Both TBCs were characterised by a structure that is typical for plasma sprayed ceramic powders. The presence of so-called *droplets* is visible, where the droplets are powder particles that have congealed on the sprayed surface, and these droplets have a flattened shape, due to impact with a liquid drop of a ceramic phase.

The phase composition of the layers was evaluated by the XRD and EBSD methods. These techniques complemented each other and did not affect the structure of the TBC layers (Fig. 4). The "macro" assessment (XRD) and micro assessment (EBSD) of the phase composition revealed the one-phase nature of the obtained layer, based on the $Nd_2Zr_2O_7$ phase with a

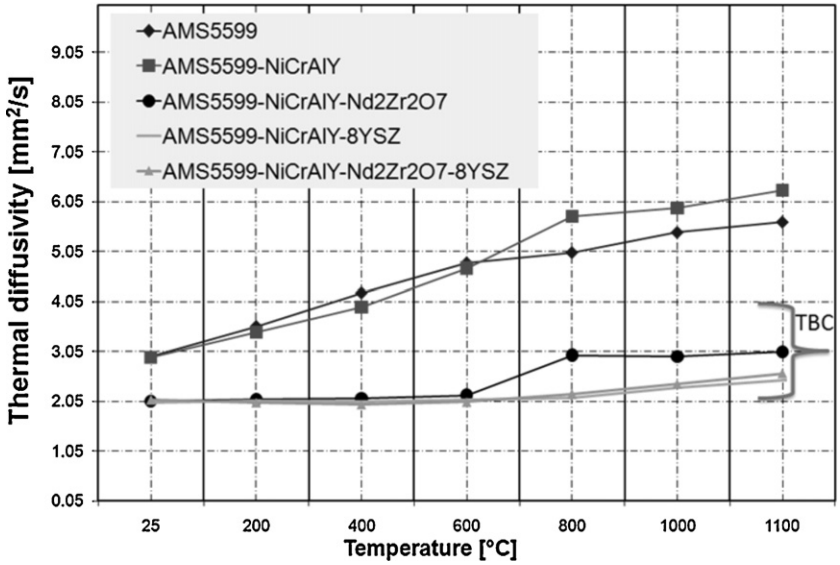

Fig. 7. Results from the thermal diffusivity measurements of the TBC layers, types 8YSZ, $Nd_2Zr_2O_7$ and $Nd_2Zr_2O_7$/8YSZ, which is measured as a monolithic system.

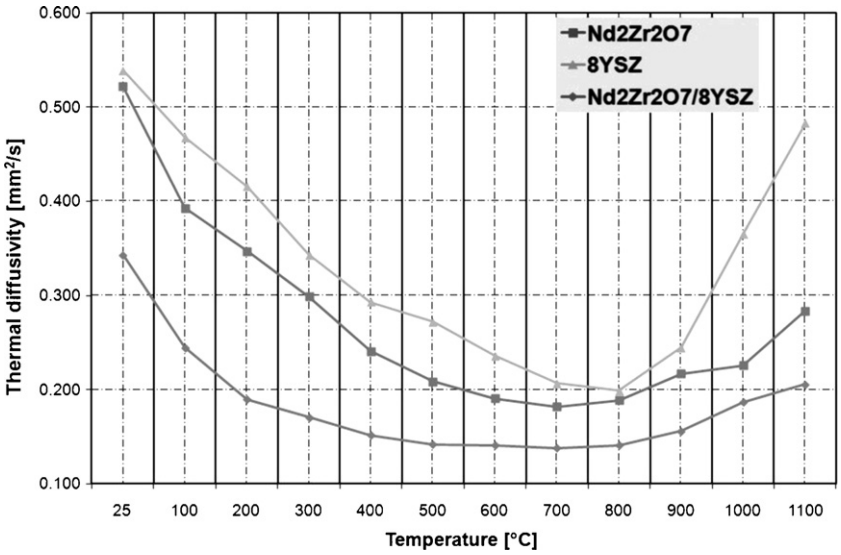

Fig. 8. Thermal diffusivity of ceramic top coat of 8YSZ, $Nd_2Zr_2O_7$ and $Nd_2Zr_2O_7$/8YSZ types obtained from two-layers model with contact resistance.

pyrochlore-type lattice (Fd3m), which is an advantageous phenomenon. The one-phase nature of the plasma sprayed layer is an extraordinary and essential feature and allows the possibility that phase transformations have a negligibly small influence on the durability of the TBC layers subjected to high operating temperatures.

The stresses occurring in the ceramic layer can be estimated from the XRD tests. Using the $\sin^2\psi$ method to analyse the stresses, values of −15 MPa and −12 MPa were estimated for the $Gd_2Zr_2O_7$ monolayer and DCL coating, respectively.

The thickness of a particular layer is a fundamental parameter and is important to determine for thermally sprayed layers and thermal barrier coatings. The thickness measurement results for the NiCrAlY prime layer and the $Nd_2Zr_2O_7$ and $Nd_2Zr_2O_7$/8YSZ ceramic layers are presented in Table 2, and a general view of the TBC layers is shown in Fig. 5. The thickness of both layers did not exceed 300 μm, and the homogeneous layer was approx. 60 μm thinner. Measurements were carried out on randomly selected images in different places on a flat sample. A number of measurements were 50, which warrants statistic corrections to the results.

Characterising the porosity of the ceramic layer was the last stage in evaluating the microstructure. Quantitative calculations of the amount of pores and cracks and the presence of so-called mass porosity, which is an unfavourable phenomenon, is usually seen. The void characteristics of the analysed layers are given in Table 3. The percentage of pores does not exceed 4.5% of the total porosity, and the percentages of individual types of pores have similar results. The DCL layers have similar values. Quantitative and qualitative pore characteristics demonstrate the predominance of spherical and horizontal pores, which favours better thermal properties of this layer. The effect of vertical

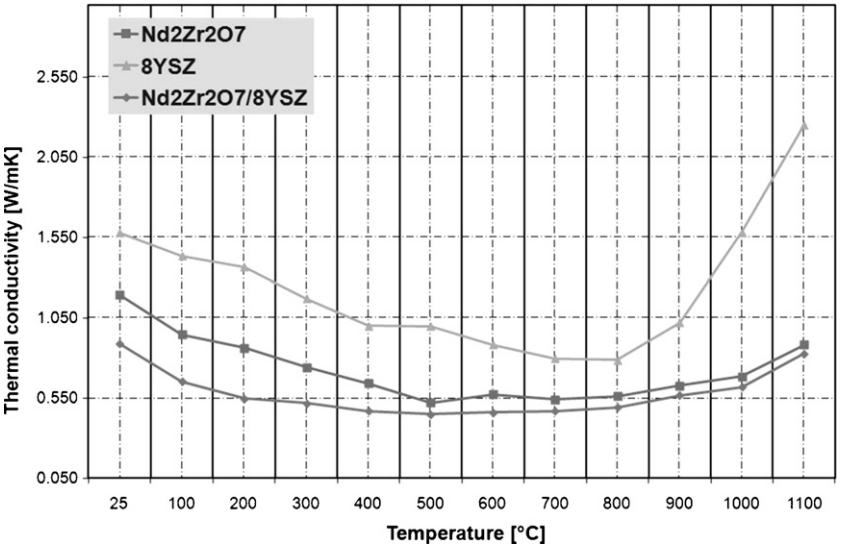

Fig. 9. Thermal conductivity of ceramic top coat of 8YSZ, $Nd_2Zr_2O_7$ and $Nd_2Zr_2O_7$/8YSZ types. Thermal diffusivity results for the TBC layers 8YSZ and $Nd_2Zr_2O_7$, measured as a monolithic system.

Table 3
Results from the evaluation of the structure of cracks and pores in the TBC layers.

	$Nd_2Zr_2O_7$	$Nd_2Zr_2O_7$/8YSZ
Total porosity [%]	4.55	4.92
Vertical pores [%]	0.19	0.23
Horizontal pores[%]	1.83	2.01
Spherical pores [%]	2.53	2.68
Av. length of horizontal pores [μm]	7.33	8.11
Av. thickness of horizontal pores [μm]	2.34	2.94
Ratio of length to thickness of horizon. pores	3.13	2.76

pores is negligibly small. These values are typical for ceramic layers that are plasma sprayed at standard process parameters. An analysis of the microstructure also revealed areas that have mass porosity. Example exemplary microstructures of both types of layers are presented in Fig. 6.

The typical microstructure of plasma sprayed barrier coating layers consists of flattened particles that are parallel to the base; interparticle voids, oriented perpendicularly to the direction of heat stream flow; and interparticle cracks, formed during the cooling process of the sprayed particles. These microcracks propagate perpendicularly to the base. Considering questions that arise due to porosity in the ceramic layer, one can state that the reduction in thermal conductivity is mainly related to the volume percentages and sizes of the pores.[20] The thermal conductivity of the gases found in the barrier layer coating pores is close to the thermal conductivity of free gases. The value in air is approx. $0.025\,Wm^{-1}\,K^{-1}$ and points to the fact that the sizes of the pores are much bigger than the mean free path. If the pore size is less than the mean free path, then the value of the thermal conductivity drops below the typical free gas value, and this behaviour is related exclusively to Knudsen's conductivity. The sizes of the pores (and grains as well) also are important for radiational heat transport because grain boundaries and similar microstructural elements have the ability to scatter the radiational component. Fine-grained structures and fine-pore structures reveal a strong tendency to scatter the heat stream and reduce the ability to emit infrared radiation.[20] Grain boundaries are the second microstructural element that determine the insulative properties of the sprayed layers. Scattering of phonons at the grain boundaries can lower the thermal conductivity at low temperatures by reducing the phonon mean free path in the sprayed layer. This effect is stable, even at high temperatures.[21,22]

Thermal diffusivity test results for the analysed materials are presented in Fig. 7.

Applying an outer ceramic layer of both types, i.e., $Nd_2Zr_2O_7$ and $Nd_2Zr_2O_7$/8YSZ, lowered the thermal diffusivity value of the AMS5599-NiCrAlY bisystem. These results demonstrate that the best effect was obtained for the 8YSZ conventional coating. However, these results do not consider the real thickness of the ceramic layer. In order to account for this thickness, it is necessary to determine the thermal diffusivity of the ceramic layers alone with the use of proper mathematical models; this method makes the results independent of the thickness of the analysed layer. The Proteus program was applied for this purpose, and the calculated data yielded thickness values of the tested layers as 240 and 300 μm for the $Nd_2Zr_2O_7$ and $Nd_2Zr_2O_7$/8YSZ coatings, respectively. A conventional layer is 300 μm thick. The bilayer model was used to calculate the thermal diffusivity of the ceramic layers, while the base material coupled with an interlayer was treated as the base material, and the outer ceramic layer was treated as an unknown material. The thermal diffusivity results, shown in Fig. 8, point to a lower value for the DCL $Nd_2Zr_2O_7$/8YSZ coating, and this behaviour is due to the properties of the charge material, the microstructure of the layer (porosity) and, the boundary that developed between the 8YSZ and $Nd_2Zr_2O_7$ phases.

Using the results of measurements of thermal diffusivity of layers and measurements of specific heat, density and coefficient of linear extension for the feedstock powders, a value of a coefficient of thermal diffusivity of analysed ceramic layers, was calculated[18–20] (Fig. 9).

These calculations point to a lower thermal diffusivity for the TBC layers obtained from powders based on neodymium zirconate of both types. Together with an increase in temperature, the DCL–$Nd_2Zr_2O_7$/8YSZ–TBC is the best solution.

4. Conclusion

In conclusion, the TBC layers based on neodymium zirconates could be an alternative to conventional 8YSZ layers. Based on the evaluation of the microstructure, the application of standard plasma spraying process parameters enabled attaining good quality $Nd_2Zr_2O_7$ and homogeneous DLC ($Nd_2Zr_2O_7$/8YSZ) ceramic layers. The porosity of both coatings did not exceed 5%. Thermal diffusivity tests revealed, as well, that the insulative properties of the zirconate layers were better compared to those of the standard coating based on the 8YSZ oxide. Moreover, due to a developed interphase boundary in the DLC, phonon scattering effects were amplified because of a grain boundary-related component that is usually negligible.

Acknowledgement

Financial support from the Structural Funds in the Operational Program – Innovative Economy (IE OP) financed from the European Regional Development Fund – Project No. POIG.0101.02-00-015/09 is gratefully acknowledged.

References

1. Miller RA. Thermal barrier coatings for aircraft engines: history and directions. *J Therm Spray Technol* 1997;**6**:35.
2. Clarke DR, Levi CG. Materials design for the next generation thermal barrier. *Coatings Annu Rev Mater Res* 2003;**33**:383.
3. Maloney MJ. United States Patent US 6,117,560 2000.
4. Maloney MJ. United States Patent US 6,284,323 2001.
5. Subramanian R. United States Patent US 6,258,467 2001.
6. Subramanian MA, Sleight AW. Rare earths pyrochlores. In: Gschneider KA, Erying L, editors. *Handbook on the physics and chemistry of rare earths*. Oxford: Elsevier Science Publishers; 1993. p. 225.
7. Vassen R, Cao X, Tietz F, Kerkhoff G, Stoever D. $La_2Zr_2O_7$ – a new candidate for thermal barrier coatings. In: Lugscheider E, Kammer PA, editors. *Proceedings of the united thermal spray conference'99*. Verlag für Schweißen und Verwandte Verfahren: ASM International; 1999. p. 830.

8. Vassen R, Cao X, Tietz F, Basu D, Stoever D. Zirconates as new materials for thermal barrier coatings. *J Am Ceram Soc* 2000;**83**:2023.
9. Wilden J, Wank M, Steffens HD, Brune M. New thermal barrier coating system for high temperature applications. In: Coddet C, editor. *Proceedings of the 15th international thermal spray conference: thermal spray meeting the challenges of the 21st century*. Materials Park: ASM International; 1998. p. 1669–73.
10. Cao X, Vassen R, Tietz F, Jungen W, Stoever D. Thermal Stability of Lanthanum Zirconate Plasma-Sprayed Coating. *J Am Ceram Soc* 2001;**84**:2086.
11. Subramanian MA, Aravamudan G, Subba Rao GV. Oxide pyrochlores – a review. *Prog Solid State Chem* 1983;**15**:55.
12. Ding C, Xi Y, Zhang Y, Qu J, Qiao H. Thermophysical properties of plasma sprayed rare earth oxide coatings. In: Sandmeier S, Eschnauer H, Huber P, Nicoll AR, editors. *The 2nd Plasma-technik-symposium*. Wohlen: Plasma-Technik AG; 1991. p. 27.
13. Lehmann H, Pitzer D, Pracht G, Vassen R, Stöver D. Thermal conductivity and thermal expansion coefficients of the lanthanum rare-earth-element zirconate system. *J Am Ceram Soc* 2003;**86**:1338.
14. Wu J, Wei X, Padture NP, Klemens PG, Gell M, Garcia E, et al. Low-thermal-conductivity rare-earth zirconates for potential thermal-barrier-coating applications. *J Am Ceram Soc* 2002;**85**:3031.
15. Xu Q, Wei P, Wang J, WanC. Qi L, Miao H, et al. Rare-earth zirconate ceramics with fluorite structure for thermal barrier coatings. *J Am Ceram Soc* 2006;**89**:340.
16. Zhu D, Miller RA. Development of advanced low conductivity thermal barrier coatings. *Int J Appl Ceram Technol* 2004; **1**:86.
17. Moskal G. Microstructure and thermal diffusivity of RE zirconate powders for TBC system obtained by the APS method. In: Gaal DS, Gaal PS, editors. *Proceedings of the thirtieth international thermal conductivity conference. Proceedings of the eighteenth international thermal expansion symposium*. Pittsburgh: DEStech Publications, Inc.; 2010. p. 451.
18. Moskal G. Characteristics of selected thermal properties of ceramic powders type $RE_2Zr_2O_7$. IV Scientific conference. Modern technologies in surface engineering. *Inzynieria Materiałowa* 2010;**4**:1107–12, in polish.
19. Moskal G, Iwaniak A, Rozmysłowska-Grund A. Characterization of Thermal Properties of Micro-Sized Ceramic Powders for APS Deposition of Ceramic Layers Key Eng. *Mat* 2011;**484**:152–7.
20. Golosnoy IO, Cipitria A, Clyne TW. Heat transfer through plasma-sprayed thermal barrier coatings in gas turbines: a review of recent work. *J Therm Spray Technol* 2009;**18**:809.
21. Charvat FR, Kingery WD. Thermal Conductivity: XIII, Effect of Microstructure on Conductivity of Single-Phase Ceramics. *J Am Ceram Soc* 1957;**40**:306–15.
22. Klemens PG. Thermal conductivity of zirconia. In: Wils KE, Dinwiddie RB, Graves RS, editors. *Thermal Conductivity 23*. Lancaster: Technomies Publishing Co.; 1996. p. 209–20.